Materials
Advances

rsc.li/materials-advances

ROYAL SOCIETY
OF **CHEMISTRY**

PAPER
Viola I. Birss, Cathleen M. Crudden, Zhe She *et al*.
Toll like receptor-based electrochemical sensors *via*
N-heterocyclic carbene-modified surfaces: towards
improved sensing of DNA molecules

ROYAL SOCIETY
OF CHEMISTRY

PAPER

Check for updates

Toll like receptor-based electrochemical sensors *via* N-heterocyclic carbene-modified surfaces: towards improved sensing of DNA molecules†

Dianne S. Lee, [ID] [a] Mir Pouyan Zarabadi,[a] Hridaynath Bhattacharjee,[a] Lin Qi,[b] Jennifer F. McLeod,[a] Kasra Saeedfar,[a] Ishwar Singh,[a] April Woods,[b] Anastasia Messina,[a] Viola I. Birss, [ID] *[b] Cathleen M. Crudden [ID] *[a] and Zhe She [ID] *[a]

Pathogen detection on gold surfaces using N-heterocyclic carbenes (NHCs) functionalized with amine tags along with an organic linker, bis(sulfosuccinimidyl)suberate sodium salt (BS^3) to chemically bind toll-like receptor 9 (TLR9) to gold electrodes, is reported here for the first time. TLRs are essential components of the early warning system of the human innate immune response, with TLR9 being a DNA sensing receptor that specifically detects DNA viruses. To enhance sensor consistency compared to previous literature, two distinct types of NHCs were used to minimize challenges associated with non-specific adsorption. Gold electrodes functionalized with TLRs *via* NHCs have the potential to operate as broad-spectrum biosensors, as evidenced by their ability to identify biological pathogens based on alterations in resistance and pattern recognition.

Introduction

The global threats of pandemic and epidemic outbreaks (MERS, Ebola, Zika, SARS-1, and SARS-2 (COVID)) are on the rise, driven by increased global mobility and global warming. Controlling and containing these outbreaks is extremely challenging without diagnostic biosensors capable of reliable pathogen detection.[1,2] Detection, identification, and monitoring capabilities are the key aspects of any biosensing system.

While sensing transducers such as surface plasmon resonance (SPR)[3,4] and quartz crystal microbalance (QCM)[5] are often employed with the biological recognition elements (BRE), electrochemical methods are more convenient due to their compact size, robustness, low power consumption, and low cost.[6,7] Common BREs include nucleic acids[8–10] and proteins,[11–13] and their use in sensors provides accurate detection of pathogens with great specificity and sensitivity. However, highly optimized and single pathogen specific sensors do not detect a breadth of analytes. This approach is not suited for applications where the pathogen is unknown.

A unique class of proteins called toll-like receptors (TLRs) are rare among BREs as they can detect various classes of

biological pathogens using a pattern recognition approach, allowing for the identification of key conserved structures present in pathogen classes.[14] For instance, TLR4 identifies lipopolysaccharide (LPS), TLR5 recognizes flagellin, TLR7 recognizes single-stranded RNA, and TLR9 recognizes and binds to DNA fragments belonging to a foreign DNA derived from bacteria and viruses.[15,16] The utilization of a single sensor decorated with different TLR BREs will be significant for the identification of unknown pathogens.[17,18]

The robustness of such sensors under different environmental and chemical conditions, the sensitivity that can be achieved, and the ability to store the sensors without loss of activity are key issues for their further development.[19–21] Most electrochemical BRE-on-metal sensors are typically fabricated by employing thiol-based self-assembled monolayers (SAMs) to link the BRE to the underlying electrode, typically gold, and enable the translation of pathogen recognition into a readable signal.[11,17] However, commonly employed thiol SAMs are known to degrade even under ambient conditions,[22] effectively limiting their use to laboratory environments.

Recent discoveries have shown that N-heterocyclic carbenes (NHCs) bind to metals *via* strong carbon-to-metal bonds, providing a highly robust linkage to the surface.[23–25] This led to the development of an antibody-based NHC-SAM sensor for the measles virus (Fig. 1a), showing exceptional response and stability.[26] In 2021, we described the first example of an NHC linked TLR-based pathogen detection system (Fig. 1b) using a similar strategy of Michael addition as described by Workentin

[a] Department of Chemistry, Queen's University, Kingston, Ontario, K7L 3N6, Canada. E-mail: zhe.she@queensu.ca

[b] Department of Chemistry, University of Calgary, Calgary, Alberta, T2N 1N4, Canada
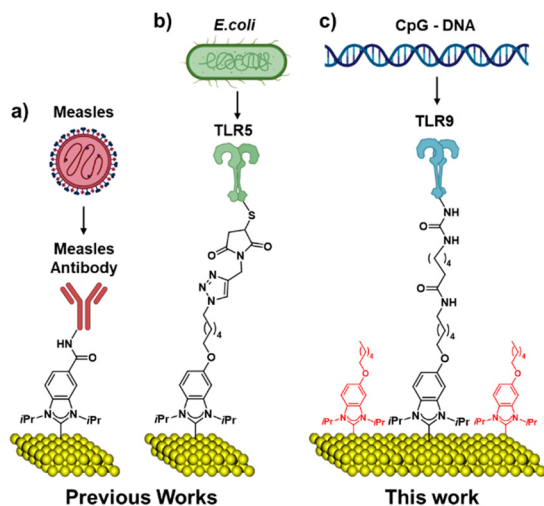
Fig. 1 Previous TLR-based biosensors based on NHC SAMs (a) for measles detection using a bound antibody, (b) for the detection of *E. coli* using TLR5, and (c) showing the new platform for surface attachment of TLR9.

and co-workers on gold nanoparticles.[27,28] Although effective, the use of an NHC with a maleimide end group for immobilization of the TLR protein moiety through Michael addition reaction required the use of thiol nucleophiles that provided a point of potential instability due to reversible reactions.[27,29] Despite the current precedents, such as DNA hybridization,[30–32] nanobeads,[33] or a reverse method of using DNA platform to detect proteins,[34] there has not yet been a reported example of electrochemical biosensors using organic ligand SAM technology along with TLRs to detect DNA molecules.

Here, we report a secure and faster strategy to build TLR-based sensors on gold surfaces (Fig. 1c), employing amide couplings to react an amine-containing NHC with TLR9 *via* a homo-bifunctional crosslinker, bis(sulfosuccinimidyl)suberate sodium salt (BS³).[35] BS³ is known to bind irreversibly to its conjugate molecules and is incorporated into this sensor design in the hopes of securely binding the NHCs and TLRs together, resulting in a very stable sensor platform. The time required for protein immobilization has been significantly lowered from 72 h to 24 h as a result of this improved binding strategy in comparison with previous reports. His-tag modification is not needed for the new strategy, which makes this new design simpler for a wide range of applications. Although BS³ was employed in this study, any crosslinker molecule allowing amide couplings may theoretically be utilized with the sensor system described in this work to tailor the monolayer thickness without having to synthesize alternative NHC molecules.

Furthermore, we also report a new strategy for lowering the risks of non-specific adsorption while minimizing unreacted substrate exposure by using two distinct NHCs. The present study shows significant improvements over prior work,[27] including its shorter synthetic route with better overall yield as well as better sensor design and replicability. The new molecule and sensor design also enables more selective detection of TLR9-based agonists.

Results and discussion

The synthesis of amine tagged NHC precursor **2** builds on the known preparation of NHC precursor **1**, which has a terminal azide group. **1** was prepared according to the published procedure (Fig. 2a),[27] then reduced to the desired amine (**2**) by a Staudinger reaction with PPh_3 in refluxing THF/H_2O (Fig. 1a and ESI†).[36] SAMs from NHC **2** were then formed by immersing cleaned gold surfaces in a 10 mM methanolic solution of NHC precursor **2** for 44 h. The NHC SAMs (**2/Au**) were interrogated by cyclic voltammetry (CV) in an electrolyte solution containing 5 mM/5 mM $Fe(CN)_6^{3-/4-}$ as the redox couple, as shown in Fig. 2b. Initially, the bare gold surface shows the highest oxidation and reduction currents with a peak separation of approximately 75 mV in 1 M $NaClO_4$. After NHC SAM formation, the redox peaks are notably suppressed, and the peak separation widens.

SAMs of **2** on Au were also characterized using high-resolution X-ray photoelectron spectroscopy (XPS). As seen in Fig. 2c, the C 1s region indicates the presence of aliphatic carbon along with C–N, C–O, and C=C species. The N 1s region provides conclusive evidence for the presence of NHC on the surface. Consistent with what has been previously reported for NHC SAMs, the N 1s XPS region in Fig. 2d was characterized by two peaks in an approximately 2:1 ratio at 401.3 eV and 399.5 eV, respectively, assigned to bound NHC and amine functional groups.

Prior to the introduction of the TLR, the NHC SAM is back-filled with NHC precursor **3** to block any gaps on the surface
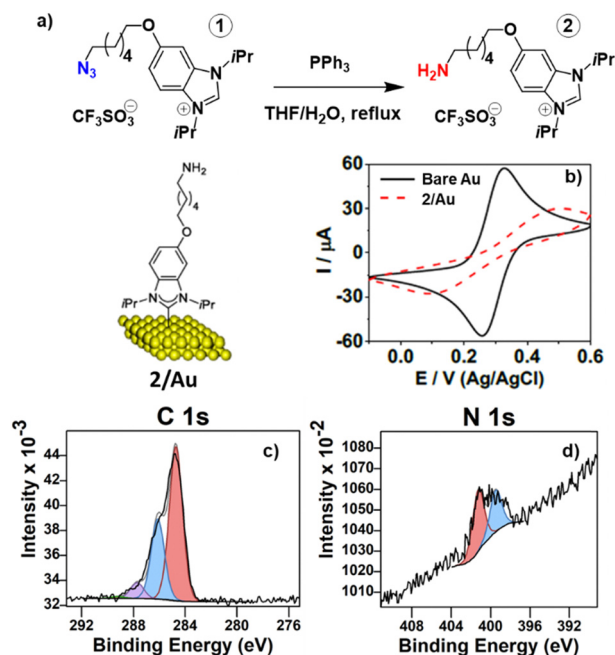

Fig. 2 (a) Synthesis of NHC **2**. Reduction of azide to amine *via* the Staudinger reaction. (b) Cyclic voltammograms (100 mV s⁻¹) of bare Au and an Au surface functionalized with **2**. The CV was collected using 5 mM/5 mM $Fe(CN)_6^{3-/4-}$ as the redox couple and 1 M $NaClO_4$ as the supporting electrolyte. Peak-fitted-high-resolution XPS of the functionalized surface (**2/Au**, left), showing the (c) C 1s and (d) N 1s regions.
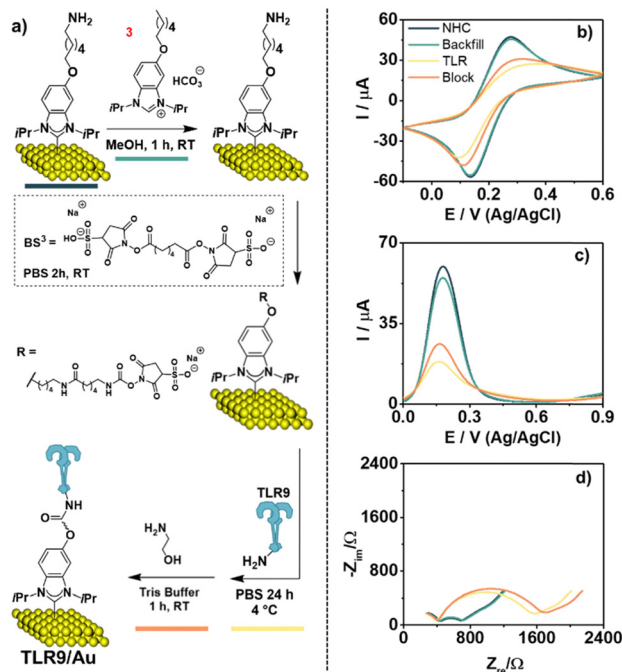
Fig. 3 (a) Schematic of the NHC biosensor construction (left). Right: (b) cyclic voltammetry (CV), (c) square wave voltammetry (SWV), and (d) electrochemical impedance spectroscopy (EIS) of each sensor construction stage, shown on the left. All electrochemical data were collected in a 10 mM HEPES aqueous buffer solution (pH ∼7.4) containing 5 mM/5 mM $Fe(CN)_6^{3-/4-}$ and 0.01 M $NaClO_4$ as the supporting electrolyte. The CVs were obtained using a scan rate of 0.1 V s^{-1} and impedance results were recorded at the open circuit potential (0.209 V $vs.$ 3M Ag/AgCl) from 100 kHz to 0.5 Hz.

and minimize non-specific adsorption that may lead to a "false positive" response (Fig. 3a).[37–39] While we typically find that NHC-based SAMs are dense packed‡, this procedure addresses the possibility of defects left by physisorption of NHC **2** through the primary amine.

The modified surface was then exposed to a solution of BS^3 in phosphate buffer saline (PBS) for 2 h at room temperature. Next, we treated the surface with a PBS solution of TLR9 at 4 °C. TLRs possess readily available primary amines found in the amino acid residues and the N-terminus of each polypeptide chain.[40] Any remaining succinimide esters were then deactivated with ethanolamine in Tris buffer for 1 h at room temperature. This deactivation process, also known as the blocking stage, prevents chemical derivatization of the sensor by the analyte, reducing the possibility of a false positive response and increasing the specificity of analyte interactions with the BRE.[37]

After each stage of sensor modification, the surface was examined by CV, square wave voltammetry (SWV), and electrochemical impedance spectroscopy (EIS) (Fig. 3). These analyses demonstrate that the suppression of current output takes place at each step of surface functionalization. Fig. 3d shows the Nyquist plots for the modified gold electrodes at each stage of

surface functionalization, where an increase in charge transfer resistance (R_{ct}) was observed in each case, but the largest increase in seen after the attachment of TLR9, with the insertion of the blocker then making little difference. Creating sensors with identical resistance baselines is a challenge associated when employing self-assembled systems. Therefore, we chose to employ normalized detection signals from triplicate runs to understand biosensor reproducibility.

Biosensing experiments were performed on the resulting TLR9 sensor, employing cytosine–phosphorothioate–guanine oligodeoxynucleotide (CpG ODN) type B, an agonist of TLR9, as the analyte.[15] The increase in R_{ct} as the concentration of CpG increases confirmed the response of the sensor to the analyte, which in this case is known to induce dimerization of TLR9 (Fig. 4a).[41] We envision this dimerization to be enabled through the flexibility of the alkyl chain and BS3 unit binding the TLR to the surface. As shown in Fig. 4b, the normalized responses (ΔR_{ct}%) increased as the concentration of CpG increased (16 ± 4%, 25 ± 6%, and 36 ± 8%). Overall, the limit of detection (LOD) of the sensor **TLR9/Au** was found to be 5 μg mL^{-1}, with a p-value of 0.007, indicating a statistically significant difference from the sensor measurement before exposure. We also tested the performance of the sensor with CpG after its storage in PBS solution at 4 °C for four weeks (Fig. 5a).[21] The sensor showed no loss in response compared to the freshly prepared versions (p-value > 0.05).

Next, we compared our **TLR9/Au** NHC-based sensor with a traditional thiol-based **TLR9/Au** sensor in which TLR9 was immobilized to Au using 1-lipoic acid n-hydroxysuccinimide ester SAM^{21} (Scheme S2, ESI†). While both the thiol and NHC linker molecules immobilize TLR9 proteins via the same amide-coupling reaction, the two linker molecules have significant different headgroups, SAM density and chain lengths. After TLR9 immobilization, ethanolamine was used to deactivate any of the remaining succinimide ester as a blocking stage, same steps used to construct **TLR9/Au** sensor. At this stage, a considerable drop in the impedance was detected for the thiolate SAM, suggesting TLR9 loss from the surface. Since thiolate-based SAMs have previously been reported for the immobilization of related proteins, we suspect that the reduced
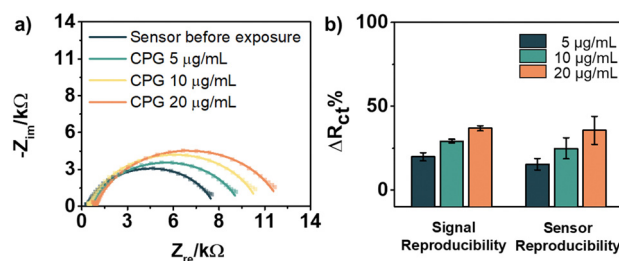

Fig. 4 (a) EIS Nyquist plots for different concentrations of CpG exposure (scatter (experimental); line (simulated)). (b) Average ΔR_{ct}% value for three measurements at one electrode after exposure to different concentrations of CpG and the average ΔR_{ct}% of three electrodes. The error bars represent the standard deviation based on the three measurement replicates per electrode and three electrode replicates for the average.
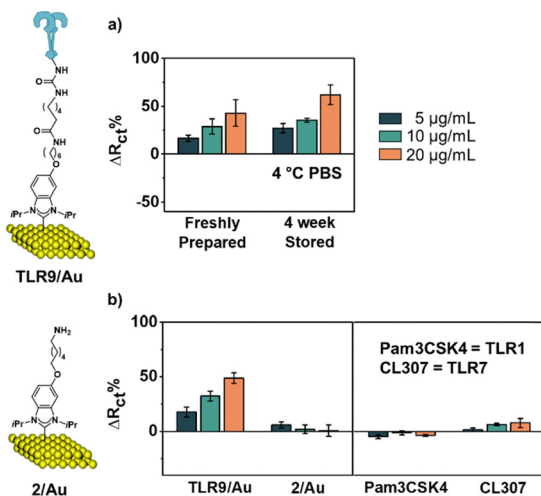
---

‡ Although the direct measurement of NHC density was not carried out in this study, prior work has estimated the coverage as $ca.$ 3–3.5 molecules nm^{-2}.[23,42]

Fig. 5 (a) Comparison of the normalized responses ($\Delta R_{ct}\%$) of freshly prepared sensor and 4-week stored sensor. (b) Comparison of $\Delta R_{ct}\%$ of **TLR9/Au** and **2/Au** towards CpG at increasing concentrations and towards different contaminants compared to the sample response to CpG. The error bars in (a) and (b) represent the standard deviation of the values obtained at three different sensors "**TLR9/Au**" and repeated measurements for "**2/Au**, Pam3CSK4 and CL307".

time for chemisorption of TLR9 to the modified surface (24 h *vs.* 72 h in prior studies[21]) may result in incomplete chemisorption onto thiol-based SAMs. The higher end group density typical in thiolate-SAMs may hinder complete reaction at these shorter reaction times. Consistent with this, after treatment with ethanolamine, the resistance (R_{ct}) of the thiol-TLR9 surface returns to the value obtained prior to TLR introduction.

For the thiol-based sensor, a negligible change in the R_{ct} signal was observed after exposure to the analyte. Together with the higher resistance of the baseline, this yielded much smaller $\Delta R_{ct}\%$ value of 0.2 ± 6, 1 ± 3, and $-3 \pm 6\%$ for CpG concentrations of 5, 10, and 20 µg mL^{-1}, respectively (Fig. S5, ESI†). Overall, these results show that the NHC-based sensor has superior TLR9-based sensor capabilities than traditional thiol systems, with NHC-based SAMs requiring less optimization to achieve comparable or improved results.[38,39]

To verify the specificity of our NHC sensor **TLR9/Au**, a control experiment was performed with **2/Au** for comparison. As shown in Fig. 5b, 2/Au produced low $\Delta R_{ct}\%$, ranging from $5 \pm 3\%$, $2 \pm 4\%$, and $0.7 \pm 5\%$, based on the three repeat measurements. On the other hand, the TLR-containing sensor showed a more reliable and positive response to CpG. For all of the CpG concentrations examined, the calculated *p*-values were found to be less than 0.05, indicating that the response contrast between the sensor and **2/Au** is significantly different (Table S1, ESI†). This control study demonstrated the importance of having TLR9 on the surface for effective recognition of CpG.

The sensor was also examined against other types of TLR agonists to confirm its specificity. For this study, TLR1 and TLR7's agonists, Pam3CSK4 and CL307, were used. In all cases, the sensor showed insignificant responses toward the other agonists (*p*-value < 0.05). Additionally, these results

demonstrated that non-specific adsorption of the other agonists did not occur, as the R_{ct} would then have increased significantly, giving a false positive.§ This is very promising for the use of this sensor in real-world settings for CpG-specific performance.

Experimental

Materials and methods

Reactions were performed with reagent grade solvents with the exception of CH_2Cl_2 and THF, which were distilled from calcium hydride and sodium benzophenone ketyl, respectively, under an argon atmosphere prior to use. 4-Amino-3-nitrophenol was purchased from Alfa Aesar, while trifluoromethanesulfonyl anhydride, chloroform-*d*, methylene chloride-*d*$_2$ acetonitrile-*d*$_3$, and methanol-*d*$_4$ were purchased from Sigma-Aldrich. CpG oligodeoxynucleotides mouse sequence type b was purchased from Novus Biologicals. NHC **3** was synthesized following a previously published procedure.[42]

Nuclear magnetic resonance (NMR) spectroscopy. ^1H, ^{13}C, and ^{19}F NMR spectra were recorded on Bruker instruments (Neo-500 and Neo-700) operating at denoted spectrometer frequency given in megahertz (MHz) at 25 °C. 1H chemical shifts are referenced to the residual protons of the deuterated solvents CDCl$_3$ (at $\delta = 7.26$ ppm) and CD$_3$OD (at $\delta = 3.31$ ppm); ^{13}C chemical shifts are referenced to the CDCl$_3$ and CD$_3$OD signals at $\delta = 77.16$ and 49.00 ppm, respectively.[43] ^{19}F NMR spectra were calibrated using CFCl$_3$ ($\delta = 0.0$ ppm) as an external reference. The following abbreviations are used to describe NMR signals: s = singlet, d = doublet, t = triplet, q = quartet, sept = septet, and m = multiplet. Coupling constants obtained from ^1H NMR spectra are associated with an error and reported to the first decimal point (the digital resolution in ^1H NMR spectra and ^{13}C NMR is 0.11 Hz and 0.64 Hz respectively). Assignments for newly synthesized compounds were supported by additional NMR experiments (COSY, HSQC, and HMBC). All data were processed using MestReNova 11.0 software.

Electrochemical experiments. All electrochemical measurements were done with a CHI6055E electrochemical analyzer potentiostat. All electrochemical experiments were performed using a three-electrode electrochemical cell with a 2 mm diameter gold disk working electrode, Ag/AgCl in 3 M KCl reference electrode, and a platinum wire as the counter/auxiliary electrode. A salt bridge was used to allow the free flow of ions from one cell to the other. The salt bridge was built using a 4 mm glass rod filled with a heated 2% agar solution in 1 M KNO$_3$ (w v^{-1}) and was stored in 1 M KNO$_3$ solution. All electrochemical data were processed with ZSimpWin and OriginPro 2016 software. Impedance measurements were all made at the open circuit potential in 5 mM/5 mM Fe(CN)$_6$$^{3-/4-}$ solution, using a 5 mV ac amplitude and scanning the frequency from 100 kHz to 0.5 Hz.

---

§ Negative $\Delta R_{ct}\%$ value means the sensor baseline R_{ct} was reduced possible due to some non-specific interactions. However, statistical test shows that the changes triggered by the agonists (control) are statistically insignificant with p-value < 0.05.

X-ray photoelectron spectroscopy (XPS). XPS spectra were recorded on a Kratos Nova AXIS spectrometer equipped with an AlN X-ray source and an MCP stack as well as a delay-line detector. The samples were mounted on an aluminium sample holder using double-sided adhesive copper tape and kept under high vacuum (10^{-9} torr) overnight before analysis. Spectra were collected using Al K_α radiation at 1486.69 eV (150 W, 15 kV) with a 10 mA emission current, a coaxial low energy electron source for charge neutralization, and a delay-line detector containing three multichannel plates. The acquisition was done using ESCape software and the data were processed in CasaXPS and MATLAB. The binding energies were charge corrected to Au $4f_{7/2}$ at 84 eV using gold samples. Shirley type background correction was applied to all high-resolution spectra.

Synthetic procedures

The key compound **1** was synthesized following the published procedure (Scheme S1, ESI†).[27]

General procedure for synthesis of NHC 2. PPh$_3$ (0.276 g, 1.05 mmol) and compound **1** (0.260 g, 0.526 mmol) were dissolved in a mixture of THF/H$_2$O (10/1, 11 mL). The resulting clear orange solution was refluxed in argon atmosphere for 20 h. After that, the reaction mixture was cooled down to r.t. and volatiles were removed under reduced pressure. A cloudy orange oil was obtained which was then dissolved in minimum volume of CH$_2$Cl$_2$ and triturated in hexanes (3 × 10 mL) and Et$_2$O (3 × 10 mL), consecutively. The resulting clear red oil was dissolved again in a minimum volume of CH$_2$Cl$_2$, passed through a short Celite plug, and concentrated to obtain **2** as a dark red sticky oil (0.187 g, 72%). ^{1}H NMR (500 MHz, CD$_3$CN) δ 8.83 (s, 1H, CH$_{(aromatic)}$), 7.77 (d, J = 9.2 Hz, 1H, CH$_{(aromatic)}$), 7.29 (d, J = 2.3 Hz, 1H, CH$_{(aromatic)}$), 7.25 (dd, J = 9.2, 2.3 Hz, 1H, CH$_{(aromatic)}$), 5.45 (s, 2H, NH$_2$), 4.89 (hept, J = 6.7 Hz, 2H, (CH$_3$)$_2$–CH–N), 4.11 (t, J = 6.6 Hz, 2H, O–CH$_2$), 2.61 (t, J = 6.5 Hz, 2H, H$_2$N–CH$_2$), 1.87–1.78 (m, 4H), 1.65 (d, J = 6.7 Hz, 12H, N–CH–(CH$_3$)$_2$), 1.53–1.45 (m, 2H), 1.42 (qd, J = 5.0, 2.2 Hz, 2H) ppm. ^{13}C NMR (126 MHz, CD$_3$CN) δ 159.53, 137.23, 133.37, 126.15, 123.28, 120.73, 115.40, 97.37, 69.92, 52.26, 51.82, 41.82, 31.81, 29.48, 26.95, 26.22, 21.98, 21.93 ppm. ^{19}F NMR (471 MHz, CD$_3$CN) δ –79.33 ppm. m/z calcd for C$_{19}$H$_{30}$ON$_3^+$ [M]$^+$ 318.25399, found 318.25229.

Surface functionalization

Modification of gold electrode. The organic contaminants on gold electrodes were removed by immersion in piranha solution (H$_2$SO$_4$: H$_2$O$_2$ = 3 : 1 v/v) for 30 s. The electrodes were rinsed thoroughly with Milli-Q (MQ) water. Electrode surfaces were further cleaned by mechanical polishing using a figure-eight polishing motion.[44] Different sizes of alumina powder (0.3 μm and 0.05 μm) were selected to prepare alumina suspensions in MQ water. Any retained alumina powder on the gold electrode was removed by ultrasonication in MQ water, then absolute ethanol and again MQ water, each for 10 minutes. The electrodes were further electrochemically cleaned to remove absorbed species from the polishing procedure. The electrodes were then electrochemically cleaned by running 100 CV cycles in 0.5 M KOH between 0 V and 2 V at a scan rate of 0.5 V s^{-1} and then 100 CV cycles in 0.5 M H$_2$SO$_4$ between 0 V and 1.5 V at the same scan rate.

Self-assembled monolayer (SAM) and biosensor formation. N-heterocyclic carbene (NHC) monolayers were prepared by dissolving **2** in HPLC-grade MeOH (10 mM solution). The gold substrates were immersed in this solution for 44 h at room temperature and then rinsed with MeOH. The modified substrates were then immersed in 10 mM MeOH solution of **3**, a hydrophobic alkyl NHC precursor for 1 h, then rinsed with MeOH. The modified substrates were then immersed in a solution of 5 mM BS^3 in PBS solution for 2 h at room temperature to produce an active ester, then rinsed with PBS solution. The modified substrates were then immersed in 250 μg mL^{-1} of TLR9 in PBS solution overnight at 4 °C in the fridge, and then rinsed with PBS solution. The modified substrates were then immersed in 1 M ethanolamine in 50 mM Tris (pH 8.4) for 1 h at RT, then rinsed with PBS solution before the electrochemical measurement.

Lipoic acid *n*-hydroxysuccinimide ester biosensor formation. Thiol based TLR9 biosensor was prepared following the published procedure (Scheme S2, ESI†).[17,21]

Biosensor testing. Once TLR biosensor preparation is completed, the biosensor is kept in a 10 mM HEPES aqueous buffer solution (pH ∼ 7.4) containing 5 mM/5 mM Fe(CN)$_6^{3-/4-}$ and 0.01 M NaClO$_4$ as the supporting electrolyte. Analytes CpG and control samples including Pam2CSK4 and CL307 were titrated into the HEPES buffer individually. The final concentration after the titration is used for calibrations. Signals were obtained 5 minutes after exposing the biosensor to the analyte.

NHC biosensor storage stability. NHC biosensors were prepared at gold discs according to the previously described methodology for **TLR9/Au**. The sensors were then immersed and stored in PBS solution for 4 weeks at 4 °C in the fridge, then removed and rinsed with PBS solution before the electrochemical measurements.

Conclusions

Here, we report a new synthetic approach to the preparation of an amine functionalized N-heterocyclic carbene (NHC) **2**, then attaching TLR9 protein to the NHC *via* amide coupling with the homo-bifunctional cross linker, BS.^{3} Additionally, a hydrophobic NHC, **3**, was employed to lower the risk of non-specific adsorption. The final sensor demonstrated a positive response towards the typical TLR9 agonist, CpG, introduced at concentrations of 5–20 μg mL^{-1}, which is the concentration range necessary for CpGs to activate TLR9 in the human immune response system.[45] The importance of the presence of TLR9 to achieve a reliable sensor response was demonstrated through a control study. The sensor also showed selectivity towards CpG when compared to agonists of other TLR proteins, such as Pam3CSK4 and CL307. The NHC-based sensors also demonstrated no loss of sensitivity, even after 4 weeks of storage.

Finally, the developed sensor design was compared to a similar and more traditional thiol-based sensor design, with the NHC-based sensor greatly outperforming the thiol-based sensor.

TLR9/Au sensor development and design to detect the presence of CpG DNA has various ramifications for biological and biotechnological applications. First, the method of detecting DNA molecules developed here could have potential applications as detection of therapeutic agents for a number of disorders, such as cancers,[16] allergies,[46] and infections.[15] Furthermore, our new sensor design enables the integration of various types of proteins or biomolecules with an accessible primary amine, such as antibodies, enzymes, or receptors, thus potentially broadening the range of analytes detectable by NHC-based biosensors.

Author contributions

CMC, ZS, and VB conceived the original idea. HB developed the synthesis of **2**. DL obtained and analysed the data, along with writing the original draft. KS, MZ, JM, AW and DL contributed to the development of the sensor platform. IS assisted with the analysis of XPS. LQ and AM carried out additional electrochemistry experiments to optimize the sensor design.

Conflicts of interest

There are no conflicts to declare.

Acknowledgements

Notes and references

1 F. Ramírez-Castillo, A. Loera-Muro, M. Jacques, P. Garneau, F. Avelar-González, J. Harel and A. Guerrero-Barrera, *Pathogens*, 2015, **4**, 307–334.

2 E. B. Mohsen Poursadeqiyan and M. F. Arefi, *J. Edu. Health Promot.*, 2020, **9**, 250.

3 C. M. Crudden, J. H. Horton, M. R. Narouz, Z. Li, C. A. Smith, K. Munro, C. J. Baddeley, C. R. Larrea, B. Drevniok and B. Thanabalasingam, *Nat. Commun.*, 2016, **7**, 12654.

4 M. Malmqvist, *Nature*, 1993, **361**, 186–187.

5 J. L. Casteleiro-Roca, J. L. Calvo-Rolle, M. C. Meizoso-Lopez, A. Piñón-Pazos and B. A. Rodríguez-Gómez, *Sens. Actuators, A*, 2014, **207**, 1–9.

6 A. Singh, A. Sharma, A. Ahmed, A. K. Sundramoorthy, H. Furukawa, S. Arya and A. Khosla, *Biosensors*, 2021, **11**, 336.

7 M. Sahar Sadat, F. Sarah Elizabeth and M. Sara, *Biosens. Bioelectron.*, 2021, **176**, 112905.

8 M. Pedrero, S. Campuzano and J. M. Pingarrón, *Anal. Methods*, 2011, **3**, 780–789.

9 D. Saakshi and J. Swati, *Biosens. Bioelectron.*, 2013, **41**, 54–64.

10 K. M. Abu-Salah, M. M. Zourob, F. Mouffouk, S. A. Alrokayan, M. A. Alaamery and A. A. Ansari, *Sensors*, 2015, **15**, 14539–14568.

11 R. M. Mayall, M. Renaud-Young, E. Gawron, S. Luong, S. Creager and V. I. Birss, *ACS Sens.*, 2019, **4**, 143–151.

12 K. Bonroy, F. Frederix, G. Reekmans, E. Dewolf, R. De Palma, G. Borghs, P. Declerck and B. Goddeeris, *J. Immunol. Methods*, 2006, **312**, 167–181.

13 S. Juliana Coatrini, S. Andrey Coatrini, P.-N. Mario, P. Fernando Vieira, N. O. Osvaldo and M. Luiz Henrique Caparelli, *Sensors and Actuators Reports*, 2022, **4**, 100083.

14 S. R. El-Zayat, H. Sibaii and F. A. Mannaa, *Bull. Natl. Res. Cent.*, 2019, 43.

15 A. A. Ashkar and K. L. Rosenthal, *Curr. Mol. Med.*, 2002, **2**, 545–556.

16 A. S. Sameer and S. Nissar, *BioMed Res. Int.*, 2021, 1–14.

17 Z. She, K. Topping, T. Ma, T. Zhao, W. Zhou, A. Kamal, S. Ahmadi and H.-B. Kraatz, *Anal. Chem.*, 2017, **89**, 4882–4888.

18 Z. She, K. Topping, M. H. Shamsi, N. Wang, N. W. C. Chan and H.-B. Kraatz, *Anal. Chem.*, 2015, **87**, 4218–4224.

19 G. Poirier, M. Tarlov and H. Rushmeier, *Langmuir*, 1994, **10**, 3383–3386.

20 N. T. Flynn, T. N. T. Tran, M. J. Cima and R. Langer, *Langmuir*, 2003, **19**, 10909–10915.

21 J. McLeod, C. Park, A. Cunningham, L. O'Donnell, R. S. Brown, F. Kelly and Z. She, *Analyst*, 2020, **145**, 6024–6031.

22 C. Vericat, M. E. Vela, G. Benitez, P. Carro and R. C. Salvarezza, *Chem. Soc. Rev.*, 2010, **39**, 1805.

23 C. M. Crudden, J. H. Horton, I. I. Ebralidze, O. V. Zenkina, A. B. McLean, B. Drevniok, Z. She, H.-B. Kraatz, N. J. Mosey, T. Seki, E. C. Keske, J. D. Leake, A. Rousina-Webb and G. Wu, *Nat. Chem.*, 2014, **6**, 409.

24 A. V. Zhukhovitskiy, M. J. MacLeod and J. A. Johnson, *Chem. Rev.*, 2015, **115**, 11503–11532.

25 G. Kaur, R. L. Thimes, J. P. Camden and D. M. Jenkins, *Chem. Commun.*, 2022, **58**, 13188–13197.

26 R. M. Mayall, C. A. Smith, A. S. Hyla, D. S. Lee, C. M. Crudden and V. I. Birss, *ACS Sens.*, 2020, **5**, 2747.

27 I. Singh, D. S. Lee, S. Huang, H. Bhattacharjee, W. Xu, J. F. McLeod, C. M. Crudden and Z. She, *Chem. Commun.*, 2021, **57**, 8421.

28 M. Workentin and P. Gobbo, *Synlett*, 2016, 1919–1930.

29 W. Huang, X. Wu, X. Gao, Y. Yu, H. Lei, Z. Zhu, Y. Shi, Y. Chen, M. Qin, W. Wang and Y. Cao, *Nat. Chem.*, 2019, **11**, 310–319.

30 D. Kato, K. Goto, S.-I. Fujii, A. Takatsu, S. Hirono and O. Niwa, *Anal. Chem.*, 2011, **83**, 7595–7599.

31 J. J. Gooding, *Electroanalysis*, 2002, **14**, 1149–1156.

32 A. Sedighi, P. C. H. Li, I. C. Pekcevik and B. D. Gates, *ACS Nano*, 2014, **8**, 6765–6777.

33 N. Soda, Z. J. Gonzaga, A. S. Pannu, N. Kashaninejad, R. Kline, C. Salomon, N.-T. Nguyen, P. Sonar, B. H. A. Rehm and M. J. A. Shiddiky, *Cancers*, 2021, **13**, 3787.

34 D. Kang, C. Parolo, S. Sun, N. E. Ogden, F. W. Dahlquist and K. W. Plaxco, *ACS Sens.*, 2018, **3**, 1271–1275.

35 M. J. E. Fischer, Amine Coupling Through EDC/NHS: A Practical Approach, in *Surface Plasmon Resonance*, ed. N. Mol and M. Fischer, Methods in Molecular Biology, Humana Press, 2010, vol. 627, pp. 55–73.

36 M. Kleoff, J. Schwan, L. Boeser, B. Hartmayer, M. Christmann, B. Sarkar and P. Heretsch, *Org. Lett.*, 2020, **22**, 902–907.

37 J. Y. Lichtenberg, Y. Ling and S. Kim, *Sensors*, 2019, **19**, 2488.

38 Z. She, M. R. Narouz, C. A. Smith, A. MacLean, H.-P. Loock, H.-B. Kraatz and C. M. Crudden, *Chem. Commun.*, 2020, **56**, 1275–1278.

39 D. T. Nguyen, M. Freitag, M. Körsgen, S. Lamping, A. Rühling, A. H. Schaefer, M. H. Siekman, H. F. Arlinghaus, W. G. van der Wiel and F. Glorius, *Angew. Chem., Int. Ed.*, 2018, **57**, 11465–11469.

40 K. Motokawa, S. K. Hahn, T. Nakamura, H. Miyamoto and T. Shimoboji, *J. Biomed. Mater. Res., Part A*, 2006, **78A**, 459–465.

41 A. Comberlato, M. M. Koga, S. Nüssing, I. A. Parish and M. M. C. Bastings, *Nano Lett.*, 2022, **22**, 2506–2513.

42 C. M. Crudden, J. H. Horton, M. R. Narouz, Z. Li, C. A. Smith, K. Munro, C. J. Baddeley, C. R. Larrea, B. Drevniok, B. Thanabalasingam, A. B. McLean, O. V. Zenkina, I. I. Ebralidze, Z. She, H.-B. Kraatz, N. J. Mosey, L. N. Saunders and A. Yagi, *Nat. Commun.*, 2016, **7**, 12654.

43 G. R. Fulmer, A. J. M. Miller, N. H. Sherden, H. E. Gottlieb, A. Nudelman, B. M. Stoltz, J. E. Bercaw and K. I. Goldberg, *Organometallics*, 2010, **29**, 2176–2179.

44 N. Elgrishi, K. J. Rountree, B. D. McCarthy, E. S. Rountree, T. T. Eisenhart and J. L. Dempsey, *J. Chem. Educ.*, 2017, **95**, 197–206.

45 Nuvusbio, CpG Oligodeoxynucleotides Mouse NBP2-31142 **https://www.novusbio.com/PDFs2/NBP2-31142.pdf**, (accessed 05-16, 2023).

46 S. C. Gangloff and M. Guenounou, *Clin. Rev. Allergy Immunol.*, 2004, **26**, 115–125.